Machine learning force field ranking of candidate solid electrolyte interphase structures in Li-ion batteries

James M. Stevenson
Schrodinger, Inc
New York, NY 10036
james.stevenson@schrodinger.com

Garvit Agarwal
Schrodinger, Inc
New York, NY 10036
garvit.agarwal@schrodinger.com

Leif D. Jacobson
Schrodinger, Inc
Portland, OR 97204
leif.jacobson@schrodinger.com

Abstract

The Solid-Electrolyte Interphase (SEI) formed in lithium-ion batteries is a vital but poorly-understood class of materials, combining organic and inorganic components. An SEI allows a battery to function by protecting electrode materials from unwanted side reactions. We use a combination of classical sampling and a novel machine learning model to produce the first set of SEI candidate structures ranked by predicted energy, to be used in future machine learning applications and compared to experimental results. We hope that this work will be the start of a more quantitative understanding of lithium-ion battery interphases and an impetus to development of machine learning models for battery materials.

1 Introduction

The fundamental nature of a battery is that during discharge the anode must be unstable with respect to the cathode, but stable with respect to the electrolyte. In practice, the best means of stabilizing anode surfaces has been to allow the formation of a solid-electrolyte interphase (SEI), a complex passivating layer which separates the metallic lithium from the organic electrolyte. Key questions about SEIs, such as whether they are amorphous or crystalline and how Li+ moves through them, remain unanswered [1, 2] limiting the development of next-generation batteries.

An SEI is a complex chemical structure that forms over large length and time scales, and involves conductors, insulators, and redox reactions; no existing method is fully applicable to the task of simulating such a system[3]. Existing pure density functionals work well for metallic systems but tend to badly underestimate reaction barriers [4–6]. Even these fastest of the useful density functional theory (DFT) methods are much too slow to study the time and length scales of the SEI. Hybrid functionals such as wB97X that yield improved barrier heights [5] struggle with metals [7, 8] and have very poor computational scaling for periodic systems [3], leaving SEI simulation out of reach.

MLFFs promise to allow atomistic simulation with the accuracy and wide applicability of DFT, but with the fast sampling of classical force fields. Many MLFF architectures exist, including Nequip [9], ChgNet [10], MACE [11], and QRNN [12]. More traditional force fields have a fixed functional form that makes them very difficult to fit for complex systems like the SEI[1]. Multitask learning lets us train MLFFs to both pure and hybrid DFT labels simultaneously[13, 14]. It has already been demonstrated that MLFFs can predict the properties of Li metal [13] (density, lattice constant, surface energy, cohesive energy, bulk modulus, equation of state, phonon spectrum) and of organic liquids

37th Conference on Neural Information Processing Systems (NeurIPS 2023).

[15, 13]. In this work, we describe a model and sampling procedure that describes the interaction of these materials and thus permits the ranking of candidate SEI structures.

2 Methods

2.1 Reference levels of theory

Based on the results of Debnath, Dajnowicz, and Stevenson [5, 15, 13], we selected wB97X-D3BJ/def2-TZVPD as our reference level of theory for non-periodic systems and PBE-D3 in a plane wave basis as our reference level of theory for periodic systems. We also labeled a random subset of non-periodic systems with PBE-D3 to improve the information exchange between output heads in our multitask learning scheme. Unfortunately, the great expense of hybrid functionals such as wB97X-D3BJ for periodic systems means that it was not feasible to label our periodic dataset with this level of theory.

Unlike previous QRNN models, ours did not use either GFN2-xTB atomic partial charge labels or DFT dipole labels for training the electronegativity-predicting neural networks. Instead, we tested reference atomic partial charges from GFN1-xTB, GFN2-xTB, and GFN0-xTB [16–18], and found the older GFN1-xTB to be the most suitable for generating charge labels for SEI training sets, because it achieves the best compromise between accuracy and convergence across isolated and periodic systems (see Appendix).

2.2 Data sampling

As in previous work on MLFFs [12, 15, 13] we use multiple rounds of active learning for data generation to increase accuracy. This data generation is based on using the best available model to sample new geometries of relevant systems. Unlike these prior works, we have used enhanced reaction sampling using Artificial Force Induced Reactions (AFIR) [19, 20] and Nudged Elastic Band (NEB) [21] on the QRNN potential energy surface.

We used the multitask abilities of QRNN [22, 13, 14] to add a totally distinct dataset of general organic chemistry, SPICE [23], using the SPICE subset consisting of elements H, Li, C, O, F, and P and adding our own GFN1-xTB atomic partial charge labels. We observed no increase in PBE-head validation RMSE on the battery datasets when adding the SPICE data, and only an 8% increase in hybrid-head RMSE, implying that the greatly increased scope of the data did not impose a heavy cost on model capacity (unlike the addition of reaction data). This result is significant because it means that the latent space of these MLFF models contains unused capacity that can be applied to broadening chemical applicability. We recommend the use of a supplemental dataset of general organic chemistry to shape the latent space via multitask training as a part of future MLFF works[14].

We doubled the width of the hidden layers in our neural networks in order to increase our model's capacity as we added more disparate data. We used a higher-priority dataset composed only of the periodic and cluster surface reaction subset of our dataset, such that each batch was sampled half from this priority data and half from the rest of the dataset (as in rehearsal [24]). We applied decoupled weight norms[25] with the norms not included in the optimizer. Otherwise our model hyperparameters were similar to those in previous work on QRNNs [15, 13] (see Appendix).

2.3 Structure Building

The SEI in lithium ion batteries is known to form over many charge/discharge cycles, so even with a fast MD method, creating plausible SEI geometries requires enhanced sampling. We generated initial SEI candidate structures using a method newly released in the Schrodinger suite [26] as the "SEI Simulator" using OPLS4 molecular dynamics with reaction templates applied at intervals[27]. Each system starts with 700 molecules of EC and 52 ions each of Li+ and PF_6-, giving a 1 M solution with 7416 total atoms (Fig 1). Each system runs with a unique random seed

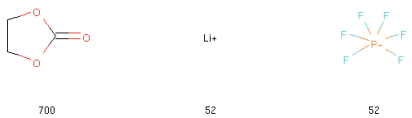

Figure 1: Initial composition of the solution of 1M $LiPF_6$ in EC solvent. Each component is labeled with its frequency in the system.

for packing and for MD, ensuring the sampling of many configurations. Some of the SEI simulator reaction templates involve adding electrons (see Appendix), which are balanced by inserting Li+ ions, producing the effect expected during SEI formation as Li+ is reduced to Li0 by electrons moving from the electrode. We defined four sets of candidates with different levels of added Li: 5, 12, 23, and 33 added Li+ ions per box (levels which arose from the SEI Simulator after 40 iterations of MD and reaction templates).

Having produced a series of unique initial geometries, we then annealed them using our reactive QRNN model with NPT MD at 400 K and 1000 atm for 100 ps each. Remarkably, our QRNN models gave stable dynamics despite the extreme conditions applied, which is often not the case for MLFFs [28]. Finally we ranked each set of candidates by calculating the mean potential energy of each structure over an MD trajectory of 20 ps length at ambient conditions of 300 K and 1 atm. Because each set of candidates has the same number of atoms of each element, the system energies are directly comparable.

3 Results

The difficulty of characterizing the SEI system experimentally is a strong motivation for this work, but also an obstacle to validation. For example, we cannot compare the density, diffusivity, viscosity, or elastic modulus of our SEI material against experimental values because such experiments do not exist for any SEI composition. Instead, we validated our model against the best available calculations for surface reaction energy barriers (see Table 1).

Table 1: Reaction barriers and reaction energies in eV for a single EC molecule on a Li (001) surface 6 layers thick (64 atoms total including EC). Note that the PBE reaction barriers (corresponding to output head 1) are much lower than the hybrid DFT barriers, as in gas phase.

	CO3 forming		Ring opening	
	ΔE barrier	ΔE rxn	ΔE barrier	ΔE rxn
PBE	0.36	-4.47	0.39	-2.65
HSE0	0.75	-4.44	0.76	-2.51
QRNN-PBE	0.28	-4.39	0.47	-2.44
QRNN-wB97	0.61	-5.03	0.69	-2.97

Assuming that our model is reasonably accurate for thermodynamically relaxed configurations of SEI-like bonds, we can use it to generate the first plausible ranking of SEI candidate structures, along with analysis of hypotheses related to SEI composition. The list of SEI candidate structures (seed*.pdb) and energies (energies.csv), along with the original 1M LiPF6 in EC solution (initial_EC_1M_LiPF6.pdb) and plotting scripts (*.py), can be found here: `https://figshare.com/s/e842ae88023902700e12`. We will refer to the lowest-energy SEI candidate structure out of the most lithiated subgroup (33 added Li atoms) as predicted by wB97X-D3BJ output head as our "best" candidate.

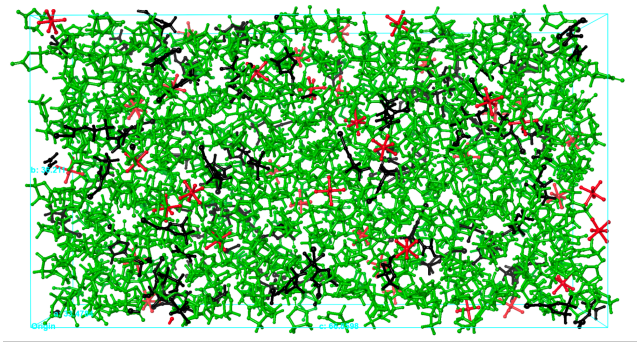

Figure 2: Our best SEI candidate structure. Green = EC solvent, red = PF_6- ions, black = new chemical compounds (see Fig:3. Note that all lithium atoms have reacted.

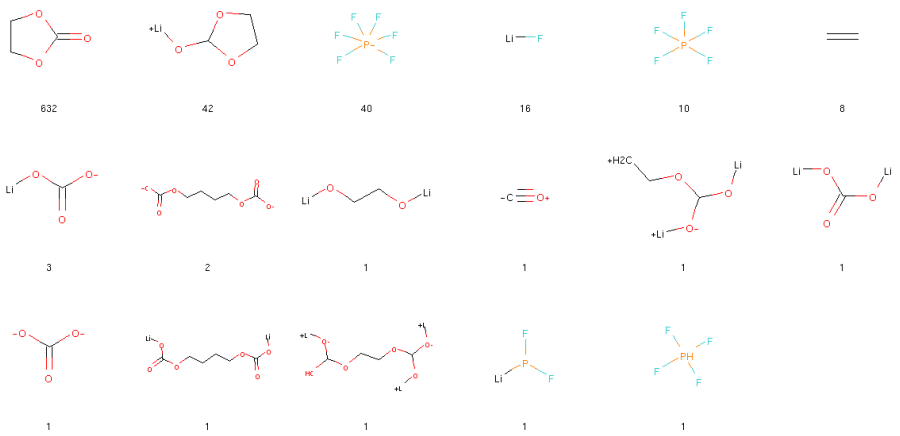

Figure 3: Final composition of our best SEI candidate. Each component is labeled with its frequency in the system. Formal charges are approximate.

We performed statistical analysis of the bonding in SEI candidate structures by recalculating the Lewis structure of the entire system based on the atomic positions after reactive MD using Schrodinger Materials Science Suite[29], then tabulating the counts of various bond types versus the total system energy (Fig 4). P-F and Li-O bonds are associated with more stable structures, while C-O and Li-F bonds are associated with less stable ones.

4 Conclusions

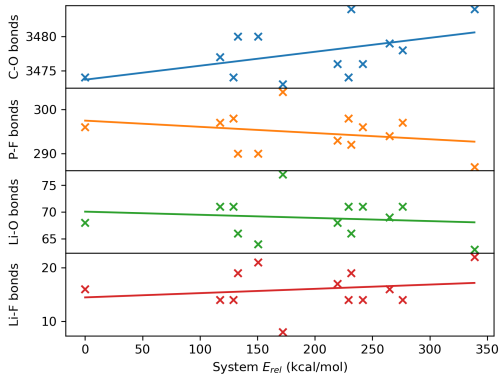

Figure 4: Bond counts with respect to total system energy (zero = most stable) for the most lithiated SEI candidate set (33 added Li+) using the wB97X-D3BJ model output.

In this work, we have demonstrated that multitask training with a QRNN model, combined with sampling of relevant chemical systems, allows a machine learning force field to model the complex reactions characteristic of an SEI. To our knowledge, this is the most complex redox reactive system simulated using an MLFF or any method of comparable accuracy.

We have so far constructed SEI candidates using only a single formulation of electrolyte, 1M $LiPF_6$ in EC. Based on this common formulation, we are able to suggest plausible structures for the SEI and analyze what makes a structure more or less energetically stable. However, the full power of this technique will come from comparing multiple formulations. Given the most stable SEI candidate for each formulation, it will be possible to calculate properties such as Li+ diffusivity and mechanical properties as a function of the starting formulation, allowing detailed optimization of SEI chemistry.

Future work should include the application of other model architectures, including Nequip and MACE [9, 11] as well as architectures which allow the use of atomic partial charges such as CHGNet [10]. Another useful technical extension of this work would be to test models trained with only subsets of the dataset used here, rather than the full dataset, to help determine which parts are most critical to

accuracy and stability of the model. Using this information, the dataset can be efficiently extended with a wider variety of reaction data.

MLFFs offer a powerful opportunity to understand SEI materials, but only if we are willing to tolerate working in an environment where theoretical and experimental references are currently limited and the probability of being proven wrong by future events is high. We hope that our contribution will be the first of many in this difficult and crucial part of materials science.

Acknowledgments and Disclosure of Funding

This work is supported and funded by Gates Ventures.

The authors declare no competing financial interest.

We would like to thank Verena Neufeld, Nongnuch Artrith, Alexander Urban, Richard A. Friesner, and the other members of the Columbia Center for Computational Electrochemistry, as well as Karl Leswing, Mat Halls, and Robert Abel of Schrodinger, Inc, and Adrian Roitberg of the University of Florida, for their advice and consultations.

References

[1] Aiping Wang, Sanket Kadam, Hong Li, Siqi Shi, and Yue Qi. Review on modeling of the anode solid electrolyte interphase (sei) for lithium-ion batteries. *npj Computational Materials*, 4(1):1–26, 2018.

[2] Kevin Leung and Katherine L Jungjohann. Spatial heterogeneities and onset of passivation breakdown at lithium anode interfaces. *The Journal of Physical Chemistry C*, 121(37):20188–20196, 2017.

[3] Joonho Lee, Adam Rettig, Xintian Feng, Evgeny Epifanovsky, and Martin Head-Gordon. Faster exact exchange for solids via occ-ri-k: Application to combinatorially optimized range-separated hybrid functionals for simple solids with pseudopotentials near the basis set limit. *Journal of chemical theory and computation*, 18(12):7336–7349, 2022.

[4] Verena A. Neufeld, Hong-Zhou Ye, and Timothy C. Berkelbach. Ground-state properties of metallic solids from ab initio coupled-cluster theory. *The Journal of Physical Chemistry Letters*, 13(32):7497–7503, 2022. doi: 10.1021/acs.jpclett.2c01828.

[5] Sibali Debnath, Verena A Neufeld, Leif D Jacobson, Benjamin Rudshteyn, John L Weber, Timothy C Berkelbach, and Richard A Friesner. Accurate quantum chemical reaction energies for lithium-mediated electrolyte decomposition and evaluation of density functional approximations. *ChemRxiv preprint*, 2023.

[6] Lars Goerigk, Andreas Hansen, Christoph Bauer, Stephan Ehrlich, Asim Najibi, and Stefan Grimme. A look at the density functional theory zoo with the advanced gmtkn55 database for general main group thermochemistry, kinetics and noncovalent interactions. *Physical Chemistry Chemical Physics*, 19(48): 32184–32215, 2017.

[7] Thomas M Henderson, Artur F Izmaylov, Gustavo E Scuseria, and Andreas Savin. The importance of middle-range hartree-fock-type exchange for hybrid density functionals. *The Journal of chemical physics*, 127(22):221103, 2007.

[8] Shaama Mallikarjun Sharada, Thomas Bligaard, Alan C Luntz, Geert-Jan Kroes, and Jens K Nørskov. Sbh10: A benchmark database of barrier heights on transition metal surfaces. *The Journal of Physical Chemistry C*, 121(36):19807–19815, 2017.

[9] Simon Batzner, Albert Musaelian, Lixin Sun, Mario Geiger, Jonathan P Mailoa, Mordechai Kornbluth, Nicola Molinari, Tess E Smidt, and Boris Kozinsky. E (3)-equivariant graph neural networks for data-efficient and accurate interatomic potentials. *Nature communications*, 13(1):2453, 2022.

[10] Bowen Deng, Peichen Zhong, KyuJung Jun, Janosh Riebesell, Kevin Han, Christopher J Bartel, and Gerbrand Ceder. Chgnet as a pretrained universal neural network potential for charge-informed atomistic modelling. *Nature Machine Intelligence*, pages 1–11, 2023.

[11] Ilyes Batatia, David P Kovacs, Gregor Simm, Christoph Ortner, and Gábor Csányi. Mace: Higher order equivariant message passing neural networks for fast and accurate force fields. *Advances in Neural Information Processing Systems*, 35:11423–11436, 2022.

[12] Leif D Jacobson, James M Stevenson, Farhad Ramezanghorbani, Delaram Ghoreishi, Karl Leswing, Edward D Harder, and Robert Abel. Transferable neural network potential energy surfaces for closed-shell organic molecules: Extension to ions. *Journal of Chemical Theory and Computation*, 18(4):2354–2366, 2022.

[13] James Minuse Stevenson, Leif D Jacobson, Garvit Agarwal, and Steven Dajnowicz. Transfer learning lithium and electrolyte potential energy surfaces from pure and hybrid DFT. In *AI for Accelerated Materials Design NeurIPS 2022 Workshop*, 2022.

[14] Leif Jacobson, James Stevenson, Farhad Ramezanghorbani, Steven Dajnowicz, and Karl Leswing. Leveraging multitask learning to improve the transferability of machine learned force fields. *ChemRxiv preprint*, 2023.

[15] Steven Dajnowicz, Garvit Agarwal, James M Stevenson, Leif D Jacobson, Farhad Ramezanghorbani, Karl Leswing, Richard A Friesner, Mathew D Halls, and Robert Abel. High-dimensional neural network potential for liquid electrolyte simulations. *The Journal of Physical Chemistry B*, 2022.

[16] Stefan Grimme, Christoph Bannwarth, and Philip Shushkov. A robust and accurate tight-binding quantum chemical method for structures, vibrational frequencies, and noncovalent interactions of large molecular systems parametrized for all spd-block elements (z= 1–86). *Journal of chemical theory and computation*, 13(5):1989–2009, 2017.

[17] Christoph Bannwarth, Sebastian Ehlert, and Stefan Grimme. GFN2-xTB — an accurate and broadly parametrized self-consistent tight-binding quantum chemical method with multipole electrostatics and density-dependent dispersion contributions. *Journal of chemical theory and computation*, 15(3):1652–1671, 2019.

[18] Philipp Pracht, Eike Caldeweyher, Sebastian Ehlert, and Stefan Grimme. A robust non-self-consistent tight-binding quantum chemistry method for large molecules. *ChemRxiv preprint*, 2019.

[19] Satoshi Maeda, Yu Harabuchi, Makito Takagi, Tetsuya Taketsugu, and Keiji Morokuma. Artificial force induced reaction (afir) method for exploring quantum chemical potential energy surfaces. *The Chemical Record*, 16(5):2232–2248, 2016.

[20] Daniel S Levine. Automatic determination of chemical reaction mechanisms with neural networks. *Second Workshop on Machine Learning and the Physical Sciences, NeurIPS 2019*, 2019.

[21] Hannes Jónsson, Greg Mills, and Karsten W Jacobsen. Nudged elastic band method for finding minimum energy paths of transitions. In *Classical and quantum dynamics in condensed phase simulations*, pages 385–404. World Scientific, 1998.

[22] Alex Kendall, Yarin Gal, and Roberto Cipolla. Multi-task learning using uncertainty to weigh losses for scene geometry and semantics. In *Proceedings of the IEEE conference on computer vision and pattern recognition*, pages 7482–7491, 2018.

[23] Peter Eastman, Pavan Kumar Behara, David L Dotson, Raimondas Galvelis, John E Herr, Josh T Horton, Yuezhi Mao, John D Chodera, Benjamin P Pritchard, Yuanqing Wang, et al. Spice, a dataset of drug-like molecules and peptides for training machine learning potentials. *Scientific Data*, 10(1):11, 2023.

[24] Anthony Robins. Catastrophic forgetting, rehearsal and pseudorehearsal. *Connection Science*, 7(2): 123–146, 1995.

[25] Tim Salimans and Durk P Kingma. Weight normalization: A simple reparameterization to accelerate training of deep neural networks. *Advances in neural information processing systems*, 29, 2016.

[26] Halls, Mathew D. Schrodinger materials science suite. `https://www.schrodinger.com/platform/materials-science`, 2023. Accessed: 2023-10-1.

[27] Norio Takenaka, Yuichi Suzuki, Hirofumi Sakai, and Masataka Nagaoka. On electrolyte-dependent formation of solid electrolyte interphase film in lithium-ion batteries: strong sensitivity to small structural difference of electrolyte molecules. *The Journal of Physical Chemistry C*, 118(20):10874–10882, 2014.

[28] Xiang Fu, Zhenghao Wu, Wujie Wang, Tian Xie, Sinan Keten, Rafael Gomez-Bombarelli, and Tommi Jaakkola. Forces are not enough: Benchmark and critical evaluation for machine learning force fields with molecular simulations. *arXiv preprint arXiv:2210.07237*, 2022. doi: 10.48550/arXiv.2210.07237.

[29] Schrodinger Python API 2023-1 documentation. schrodinger.application.matsci.nano.xtal module. `https://www.schrodinger.com/sites/default/files/s3/public/python_api/2023-1/api/schrodinger.application.matsci.nano.xtal.html`, 2023. Accessed: 2023-10-1.

[30] So Takamoto, Chikashi Shinagawa, Daisuke Motoki, Kosuke Nakago, Wenwen Li, Iori Kurata, Taku Watanabe, Yoshihiro Yayama, Hiroki Iriguchi, Yusuke Asano, et al. Towards universal neural network potential for material discovery applicable to arbitrary combination of 45 elements. *Nature Communications*, 13(1):1–11, 2022.

[31] Paolo Giannozzi, Stefano Baroni, Nicola Bonini, Matteo Calandra, Roberto Car, Carlo Cavazzoni, Davide Ceresoli, Guido L Chiarotti, Matteo Cococcioni, Ismaila Dabo, et al. Quantum espresso: a modular and open-source software project for quantum simulations of materials. *Journal of physics: Condensed matter*, 21(39):395502, 2009.

[32] John P Perdew, Kieron Burke, and Matthias Ernzerhof. Generalized gradient approximation made simple. *Physical review letters*, 77(18):3865, 1996.

[33] Stefan Grimme, Jens Antony, Stephan Ehrlich, and Helge Krieg. A consistent and accurate ab initio parametrization of density functional dispersion correction (dft-d) for the 94 elements h-pu. *The Journal of Chemical Physics*, 132(15):154104, 2010.

[34] Justin M Turney, Andrew C Simmonett, Robert M Parrish, Edward G Hohenstein, Francesco A Evangelista, Justin T Fermann, Benjamin J Mintz, Lori A Burns, Jeremiah J Wilke, Micah L Abrams, et al. Psi4: an open-source ab initio electronic structure program. *Wiley Interdisciplinary Reviews: Computational Molecular Science*, 2(4):556–565, 2012.

[35] Ehlert, Sebastian and Balduf, Ty and Bannwarth, Christoph and Grimme, Stefan. xtb-python. `https://github.com/grimme-lab/xtb-python`, 2022. Accessed: 2022-9-23.

[36] Ehlert, Sebastian and Balduf, Ty and Bannwarth, Christoph and Grimme, Stefan. tblite. `https://github.com/tblite/tblite`, 2023. Accessed: 2023-10-1.

[37] Lowik Chanussot, Abhishek Das, Siddharth Goyal, Thibaut Lavril, Muhammed Shuaibi, Morgane Riviere, Kevin Tran, Javier Heras-Domingo, Caleb Ho, Weihua Hu, et al. Open catalyst 2020 (oc20) dataset and community challenges. *Acs Catalysis*, 11(10):6059–6072, 2021.

[38] Stefan Grimme, Marcel Müller, and Andreas Hansen. A non-self-consistent tight-binding electronic structure potential in a polarized double-ζ basis set for all spd-block elements up to z= 86. *The Journal of Chemical Physics*, 158(12), 2023.

A Appendix

A.1 Training

Our loss function is the same as that used in previous QRNN works [13, 14], consisting of energy and atomic force mean squared error for each level of theory in each training batch, along with charge mean squared error in each training batch (charges are not separated into different output heads in our model, with all levels of theory using consistent charge labels).

Because of the addition of the SPICE dataset, we had four output levels of theory in total for multitask training: GFN1-xTB, PBE-D3, wB97X-D3BJ/def2-TZVPD, and finally the SPICE level of theory wB97X-D3BJ/def2-TZVPPD. Of these, the first and last output heads were only used to shape the latent space of the model during training, not for prediction on SEI systems.

As in our previous work, we used the Adamax optimizer with decoupled weight decay, which we have found to be highly stable and effective at a wide range of learning rates. For our final model we used a learning rate of 2e-3. We found little effect of early stopping validation for this dataset (likely because the model does not have enough capacity to overfit), so we used only 1% of the data (selected uniformly at random) as our validation set. We used hidden layers of size 256, 224, and 192 for all elements. Our batch size was 64. We found that a high level of weight decay, 3e-3 per batch, was helpful in producing smoother energy surfaces with faster convergence during geometry optimization, particularly the difficult geometry optimizations required for NEB, but this higher weight decay also reduced the height of our reaction barriers relative to the reference barriers, so for our final model we used a more conventional weight decay of 1e-3. Our final model was an exponential moving average of the training parameters, averaging every 10 batches with alpha = 0.001.

A.2 Data

We constructed our initial geometries for liquid systems, such as liquid EC, using Disordered System Builder [26] and equilibrated using NPT ensemble for 1 ns to obtain equilibrated density. For simulations of solid-liquid interface geometries, we started from a BCC lattice of lithium with the lattice constant optimized using the model to be used in MD (either the PBE-D3 or the wB97X-D3BJ head), placed next to the equilibrated liquid EC slab with an initial spacing of 2 Å. No constraints were applied to the lithium slab; the lithium was allowed to participate fully in the dynamics.

Because the SEI is suspected to include various lithium salts [Harrison], we have also added lithium oxide, lithium carbonate, lithium fluoride and lithium hydroxide to the training set, both in periodic and cluster geometries. In addition to the experimentally observed crystal geometries for the crystalline materials in the training set, we sampled non-equilibrium geometries by adding Gaussian noise to the Cartesian coordinates of the original geometries. A previous work [30] has shown good results from sampling from fully amorphous structures, an approach we pursued for SEI-like sampling using Schrodinger Disordered System Builder for ethylene carbonate (EC) with lithium hexafluorophosphate ($LiPF_6$). By setting the Van der Waals radius factor to 0.5, we were able to produce steric clashes that overcame reaction barriers and resulted in chemical reactions. We relaxed the candidate structures by annealing them using QRNN MD, and extracted finite-sized clusters for evaluation with gas-phase DFT.

We have not used DFT-generated MD, AFIR, or NEB geometries as training inputs, considering these expensive reference-level calculations to be too close to training on the test set. Instead, we have only used single-point DFT calculations on input geometries generated by non-DFT means.

We performed periodic DFT using Quantum Espresso[31] as implemented in Schrodinger Materials Science Suite[26] version 2022-3 with the same settings as in Stevenson et al [13]. The exchange-correlation energy was determined using generalized gradient approximation (GGA) Perdew-Burke-Ernzerhof (PBE) functional[32] with D3 dispersion correction[33] and a plane wave energy cutoff of 40 Ry. The Brillouin zone integration was performed using a 3x3x3 k-point mesh for bulk supercells and a 3x3x1 k-point mesh for the surface supercells.

We performed gas-phase wB97X-D3BJ/def2-TZVPD DFT using Psi4 v1.6 with the same settings as in Stevenson et al [34, 13]:

```
 scf_type': 'MEM_DF', 'dft_basis_tolerance': 1e-10,
'ints_tolerance': 1e-10, 'maxiter': 200, 'dft_pruning_scheme': 'robust',
's_orthogonalization': 'partialcholesky', 's_cholesky_tolerance': 1e-6
```

For NEB with periodic systems, we used lithium surfaces with 54 atoms (6 layers of 9 atoms each) topped with a single EC molecule. We focused on a relatively small part of reactive chemical space, the known decomposition reactions of EC, as the most important for the early phases of SEI formation. Likewise we did not sample these reactions on other surfaces, such as lithium oxide or lithium carbonate, which might potentially be relevant (though the barriers would be expected to be much higher). To create non-periodic systems out of this reactive data, for labeling with wB97X-D3BJ, we extracted clusters including the atoms from the reacting EC molecule and the Li surface within 3-6 Angstroms from any of these atoms.

Since the SEI structures are metalorganic solids with a network of covalent bonds, there is no unique way to determine the boundaries of each cluster as we did for small-molecule liquids by following the molecular boundaries. Therefore, we extracted the clusters by choosing a radius around each central atom from a uniform distribution from 3.0 to 5.2 Å extracting all the atoms within this radius plus a 1.2 Å buffer for hydrogen atoms only, and capping any cut bonds with hydrogen atoms.

An important avenue for future work in SEI active learning is to generate data via MD on amorphous metalorganic systems small enough to be directly labeled with DFT (fewer than 200 atoms). While not large enough to capture SEI properties, such systems might contain structural motifs not sampled by cluster-based methods, and would also provide an additional source of validation against DFT for more complex structures. We do not regard our current model as final, since its scope is still small compared to what is required.

Energy and gradient RMSEs from the final validation of training are shown below, in kcal/mol for energies and kcal/mol/Å for gradients. The GFN1-xTB head encompasses all the data, periodic and

non-periodic, including the SPICE supplemental dataset. The PBE-D3 head contains periodic data. The lithium and electrolyte cluster data is under the wB97X-D3BJ/def2-TZVPD head, while the final wB97M-D3BJ/def2-TZVPPD head is the SPICE data. RMSE and EMA_RMSE refer to the parameters with and without exponential smoothing (it is evident that the exponential smoothing is beneficial).

```
GFN1-xTB RMSE: 22.85 EMA_RMSE: 16.95 at validation 999
GFN1-xTB Gradient RMSE: 4.64 EMA_RMSE: 4.50 at validation 999
PBE-D3 RMSE: 22.59 EMA_RMSE: 15.09 at validation 999
PBE-D3 Gradient RMSE: 2.65 EMA_RMSE: 2.59 at validation 999
wB97X-D3BJ/def2-TZVPD RMSE: 10.92 EMA_RMSE: 9.74 at validation 999
wB97X-D3BJ/def2-TZVPD Gradient RMSE: 6.08 EMA_RMSE: 5.88 at validation 999
wB97M-D3BJ/def2-TZVPPD RMSE: 3.34 EMA_RMSE: 2.12 at validation 999
wB97M-D3BJ/def2-TZVPPD Gradient RMSE: 3.85 EMA_RMSE: 3.77 at validation 999
```

A.3 Grimme GFN*-xTB methods for labeling of periodic reactive systems

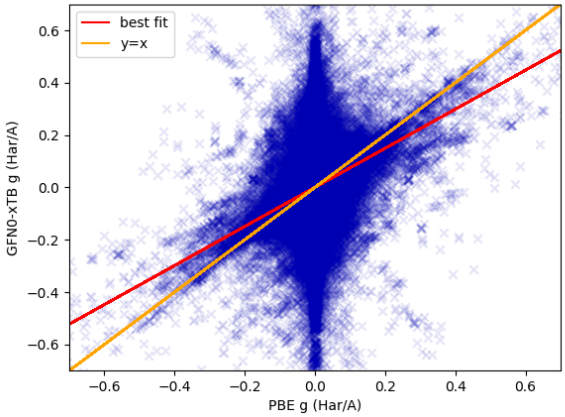

Figure 5: GFN0-xTB gradient parity plot for copper catalyst dataset. Accuracy is poor, which makes sense since this application is outside the normal scope of GFN0-xTB.

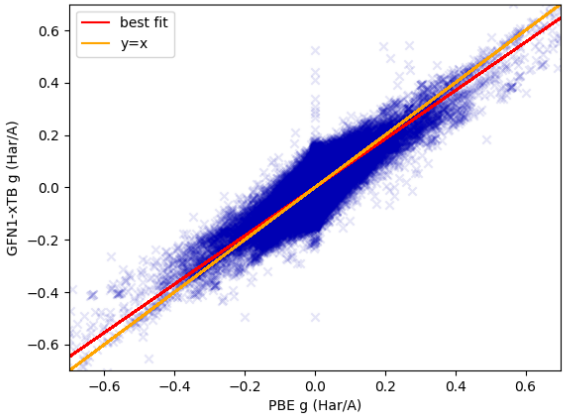

Figure 6: GFN1-xTB gradient parity plot for copper catalyst dataset. Accuracy is improved over GFN0-xTB.

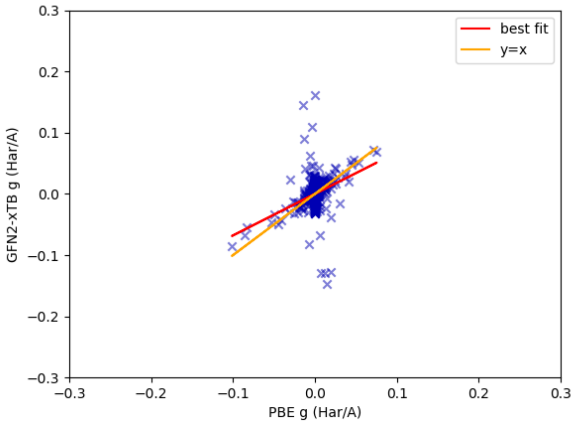

Figure 7: GFN2-xTB gradient parity plot for copper catalyst dataset. The convergence rate is very poor, such that few points are available to be plotted.

We performed GFN0-xTB, GFN1-xTB, and GFN2-xTB semiempirical calculations using the xTB python API xtb-python[35] with the default settings (accuracy 1.0, max iterations 250), except for periodic systems with GFN1 and GFN2 for which we used the tblite[36] Python API with its default settings (as of our tests, xtb-python did not support periodic boundary conditions for GFN1-xTB or GFN2-xTB). We discarded systems that did not converge, as well as any systems with NaN or infinite energies or gradients, or with very implausible partial charges (as defined by an absolute partial charge above 4 electrons/atom).

We investigated the performance of the GFN family of methods for periodic metallic surfaces using the OpenCatalyst copper surface reaction dataset [37]. We found that for this highly-challenging test set, GFN1-xTB achieved the best performance. The atomic forces from GFN0-xTB showed only a weak correlation with those of DFT, while GFN2-xTB simply did not iterate to convergence for the vast majority of the copper surface systems.

Grimme's more advanced PTB method [38] unfortunately is not yet implemented for periodic systems, so we could not use it in this comparison.

A.4 SEI Generation

x

Final composition SMILES and counts for best SEI structure from wB97X-D3BJ output head with 33 added Li atoms (formal charges are estimates):

```
'O=C1OCCO1': 632
'[Li+]OC1OCCO1': 42
'F[P-](F)(F)(F)(F)F': 40
'[Li]F': 16
'FP(F)(F)(F)F': 10
'C=C': 8
'[Li]OC1OCCO1': 6
'[Li]OC([O-])=O': 3
'[O-]C(=O)OCCCCOC([O-])=O': 2
'[Li]OCCO[Li]': 1
'[C-]#[O+]': 1
'[Li+][O]1CCOC1O': 1
'OC1OCCO1': 1
'[Li]OC(=O)OCC': 1
'[Li]OC([O-][Li+])OC[CH2+]': 1
'[Li]OC(=O)O[Li]': 1
```

	Reactions	Freq (ps)	Prob
1	$Li^+ + EC \rightarrow Li^+(EC)$	80	0.16
2	$Li^+(EC) + e^- \rightarrow$ o-LiEC	40	0.4
3	$2(\text{o-LiEC}) \rightarrow Li_2EDC + C_2H_4$	10	1.0
4	$2(\text{o-LiEC}) \rightarrow Li_2BDC$	10	1.0
5	$\text{o-LiEC} + e^- \rightarrow LiCO_3^- + C_2H_4$	80	0.5
6	$LiCO_3^- + Li^+ \rightarrow Li_2CO_3$	10	1.0
7	$LiCO_3^- + Li^+(EC) \rightarrow Li_2EDC$	10	1.0
8	$Li^+ + PF_6^- + e^- \rightarrow LiF + PF_5^-$	40	1.0
9	$Li^+ + PF_5^- + e^- \rightarrow LiF + PF_4^-$	10	1.0
10	$Li^+ + PF_4^- \rightarrow LiF + PF_3$	10	1.0

Figure 8: SEI Simulator reaction templates applied between stages of OPLS MD when applicable geometries arise and the probability criterion is satisfied.[27]

```
'[O-]C([O-])=O': 1
'[Li]OC(=O)OCCCCOC(=O)O[Li]': 1
'[Li+][O-]C(O[Li+])OCCOC([O-][Li+])O': 1
'[Li][O]([Li+])C([O-])O': 1
'[Li+][O-]([Li+])C(O)O': 1
'[Li]P(F)F': 1
'FP(F)(F)F': 1
```

Bonding is calculated using the functions connect_atoms and assign_bond_orders_w_mmlewis in the Schrodinger module schrodinger.application.matsci.nano.xtal [29].

A good avenue for future research is to include entropic contributions so as to rank the structures based on free energy. Another important next step is to run enhanced sampling for a longer time, and at higher temperatures and pressures, so as to produce more chemical reactions and a broader range of output structures. Although the energy differences between boxes are in the hundreds of kcal/mol, this is small on the scale of the thousands of atoms in each box. For example, the wB97X-D3BJ head MD with 33 added Li atoms had an energy standard deviation of 0.01 kcal/mol/atom between the candidate structures. The equivalent PBE-head MD showed a larger standard deviation of 0.02 kcal/mol/atom, which is expected considering that its lower reaction barriers should lead to broader sampling of chemical space.

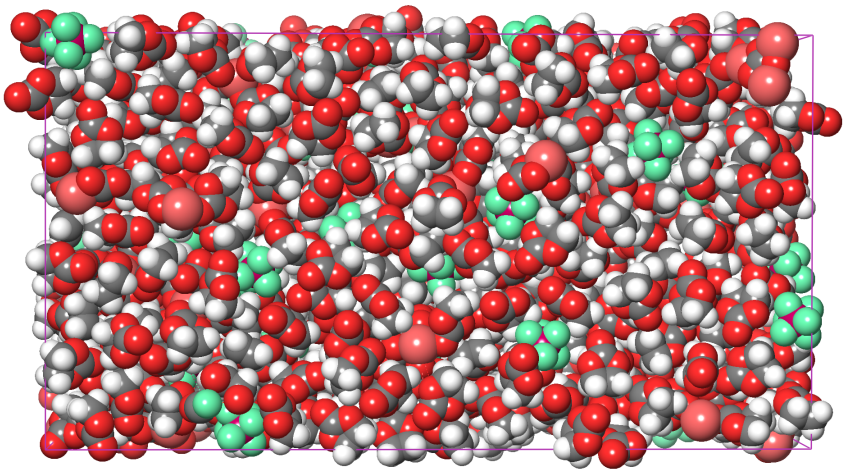

Figure 9: Our best SEI candidate structure, in Van der Waals view with atoms colored by element. 7449 atoms are present in total. Pink = lithium, red = oxygen, grey = carbon, white = hydrogen, teal = fluorine, purple = phosphorous.

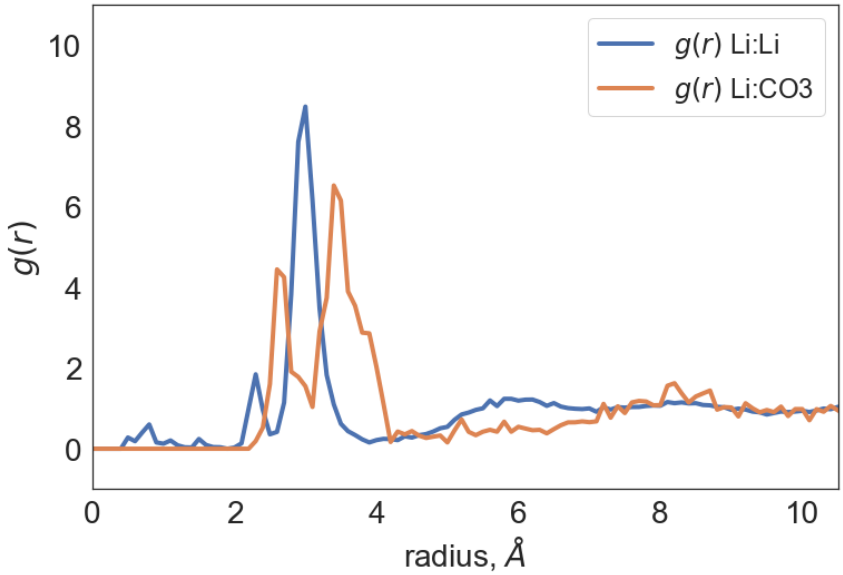

Figure 10: Radial Distribution Function (RDF) for Li and carbonate within the most stable SEI structure using the wB97X-D3BJ model output.